Construction and Building Materials 452 (2024) 138969

Contents lists available at ScienceDirect

Construction and Building Materials

journal homepage: www.elsevier.com/locate/conbuildmat

Thermal behavior of construction and demolition waste-based geopolymer

Francesca Servadei, Annalisa Natali Murri *, Elettra Papa, Valentina Medri *, Elena Landi

National Research Council - Institute of Science, Technology and Sustainability for Ceramics (CNR-ISSMC), Via Granarolo, 64, Faenza, RA 48018, Italy

ARTICLE INFO

Keywords:
Geopolymer
Construction and demolition waste (CDW)
Metakaolin
Sodium silicate
Alkali-activation
Thermal behavior
Waste recycling

ABSTRACT

Unsorted Construction and Demolition Waste (CDW) from residential building was tested as solid precursor for obtaining eco-sustainable alkali activated materials with potential applications in the building industry. Suitable reactive systems for material consolidation were tested, including alkaline solutions of sodium hydroxides and/or silicates at different concentrations. Metakaolin (MK) was also tested as an additional precursor together with CDW in different ratios to optimize geopolymerization. An MK/CDW weight ratio of 40/60 and sodium silicate as alkaline activator allowed the production of a well-reacted and cohesive material, with a bulk density of 1.35 g/cm^3, a monomodal mesoporosity with a modal pore size of 0.0214 μm (open porosity ~42 vol%), and a compressive strength of 25 MPa, thus showing similar features to those of pure metakaolin based-geopolymers. Thermal characterization was performed up to 1000°C showing that the material can exhibit thermal stability up to 650°C. Above that temperature a shrinkage due to viscous flow occurred, followed by an expansion over 750°C with the formation of macropores and dense struts. Based on these results, the developed CDW-based geopolymer has the potential for use in green building applications, with adequate thermal stability up to medium-high temperatures.

1. Introduction

The exponential growth in urbanization and industrial activities has led to an unprecedented surge in demolishing, repairing, and renovating buildings and infrastructures, resulting in the generation of massive quantities of waste. Construction and Demolition Waste (CDW) comprises the largest waste stream in the EU, accounting for more than one third of the total amount of waste produced each year [1]. Indeed, in 2020, an estimated 2.24 billion tons of solid waste were generated globally, with CDW accounting for at least 30 %. CDW levels vary by region, but China, the U.S., and the EU are the largest contributors. While recovery rates range from 7 % to 90 %, around 35 % of global CDW is sent to landfills, despite 75 % having the potential for reuse [2]. The disposal of CDW in landfills poses environmental hazards, including soil and water contamination, and resource depletion. Hence, the European Commission has established CDW as a priority waste stream for reuse, recycling and recovery [3].

Circular economy principles offer a holistic framework for addressing this challenge by promoting the reuse and recycling of waste materials such as CDW, which has an enormous transformative potential to integrate different kinds of waste materials (natural stones, aggregates, concrete rubble, bricks, ceramic scraps, reclaimed wood, polymer foams and insulating materials, etc.) into circular and sustainable solutions for building applications [2,4].The reuse and valorization of CDW involve various strategies. One of the most common approaches is processing crushed concrete and masonry to produce recycled aggregates, which can replace traditional virgin aggregates in concrete production [5–8]. Another method is manufacturing prefabricated building components, such as precast concrete elements or modular structures, using recycled materials [9,10]. Additionally, road pavements can be recycled into new asphalt mixtures through cold or hot in-place recycling [11,12]. Organic components of CDW can also be converted into green energy through anaerobic digestion or incineration processes [13,14]. However, at present, most recovered CDW is limited to low-tech applications (i.e. masonry products and road sub-bases) [15].

One of the most promising technologies proposed so far for the design and development of high-added value products within the building and construction industry is alkali-activation and geopolymer technology. This involves the chemical activation of aluminosilicate precursors with alkaline solutions, leading to the formation of three-dimensional, amorphous networks, in turn yielding robust and high-performance materials, which have garnered significant attention as sustainable alternatives to traditional cement-based materials [16–19]. Since geopolymers or more generally Alkali Activated Materials (AAMs),

* Corresponding authors.
E-mail addresses: annalisa.natalimurri@issmc.cnr.it (A. Natali Murri), valentina.medri@issmc.cnr.it (V. Medri).

https://doi.org/10.1016/j.conbuildmat.2024.138969
Received 25 June 2024; Received in revised form 23 October 2024; Accepted 27 October 2024
Available online 31 October 2024
0950-0618/© 2024 The Authors. Published by Elsevier Ltd. This is an open access article under the CC BY license (http://creativecommons.org/licenses/by/4.0/).

according to Provis's definition [20], have shown flexibility in utilizing waste and industrial by-products of various kinds as raw material [21–27], alkali activation process has a great potential to foster the green development of the building industry by reusing and valorizing CDW. Indeed, converting these wastes into geopolymer and, more in general, AAMs can promote an easy and sustainable resource management, as well as reducing carbon emissions and mitigating environmental concerns [28,29].

CDW such as waste from bricks, ceramic tiles, concrete and glass can properly act by itself as a solid precursor for the formation of AAMs, considering its chemical and mineralogical composition, which is usually rich in aluminosilicates more or less reactive in a context of alkaline activation [30,31] with only 20−30 wt% of amorphous phases [31]. The presence of additional phases such as alkaline-earth oxides, pozzolanic and hydraulic phases can also confer further properties to the geopolymeric material through the formation of hydrated and mixed phases of the C-(N)-A-S-H type by simple room-temperature reactions [29,32]. The resulting materials can have good chemical-physical properties, combined with excellent durability and enhanced mechanical performance, besides reducing the environmental burden associated with waste disposal.

Few authors [28,33–36] have explored the use of CDW as the sole aluminosilicate precursor in alkali-activated mixes to maximize CDW upcycling ratio and move one step closer to sustainable construction materials with reduced environmental impact. However, the-low-to-medium reactivity of CDW-based materials [37,38], especially when unseparated wastes are considered, requires the combined utilization of CDW together with more readily reactive precursors. Recent studies also reported the reuse of fly ash, rice husk ash, ground granulated blast furnace slags, silica fume, and metakaolin combined with CDW-based precursors into new alkali-activated construction materials, highlighting excellent mechanical properties and resistance to harsh environmental conditions for the developed materials, as well as enhanced early-age strength and reduced environmental impact compared to mixtures without CDW partially replacement [32,39–48]. In particular, slag and metakaolin allow ultimate strength to be reached before 28 days [29], while metakaolin is the most reactive in mixture design of geopolymer binders, since it forms geopolymeric networks by conventional method or along with other gehlenite-rich materials by using K-Ca compound [31].

Although extensive research has been conducted on utilizing CDW as a sustainable raw material for geopolymers and AAMs, many of the published works overlook the technological complexities involved in separating waste fractions on a large scale at CDW management and treatment plants and propose the utilization of individual ceramic and concrete fractions separated in the laboratory. There is an urgent need to find novel approaches to reuse unseparated CDW, that is difficult due to its variability. CDW has different chemical compositions based on the sources of the materials, region and construction traditions around the world, which makes it challenging to gain comprehensive insights. Moreover, limited information is available on the thermal stability of CDW-based geopolymers, which can vary significantly depending on the source and nature of the CDW used (e.g. concrete, bricks, ceramics, gypsum plaster, etc.). Some studies have investigated the thermal behavior of CDW-based geopolymers, mainly using pre-selected wastes of clay bricks, cement and concrete or ceramic tile [49–52]. CDW from tile and brick waste resists temperatures up to 1050°C [49,50], while the presence in the mixture of cementitious fractions and lime plaster can limit the structural resistance to a maximum of 500°C [52]. In light of this, our aim was to investigate alkali-activated formulations based on mixed and unsorted CDW which could exhibit a geopolymer-like microstructure and pore size distribution, and to assess their thermal behavior for applications in the building industry.

Starting from these premises, this paper explored the feasibility of preparing eco-sustainable geopolymer/ alkali-activated materials using unsorted CDW, with a view to potential application in the building industry. The demolition waste was obtained from a residential building dating to the early 1900s, without performing any fraction separation in order to develop a process potentially applicable at an industrial scale and was milled to powder. To explore its full geopolymerization potential, formulations containing various amounts of CDW as solid precursor and different alkali-activators (i.e., sodium hydroxides and/ or silicates at different concentrations) were tested. Commercial metakaolin was also introduced with CDW powder in different ratios to compensate for the partial reactivity of the waste material, thus favoring geopolymerization. The workability and effective alkali-activation of the prepared mixtures were evaluated; the physical and chemical features as well as the pore size distribution, macro- and microstructure of the resulting geopolymers, were analyzed, thus identifying among them an optimized geopolymer binder. On this binder, compression tests and thermal analysis were performed. Specimens exposed up to 1000°C were fully characterized in terms of their macro- and microstructure, pore size distribution and mineralogical composition, enabling a better understanding of the thermal behavior of CDW-metakaolin-based geopolymers.

2. Experimental procedure

2.1. Raw materials

Unsorted CDW was collected from a historical residential building (late 19th century) in the province of Bologna, Emilia Romagna region. The collected material came from the demolition of sections of solid brick masonry, cement-based mortars, lime-based binders with fine natural sand aggregate, portions of gypsum plaster, non-structural or decorative elements made of cement paste, and portions of flooring with cement binder and natural stone aggregates. The waste material was first crushed into raw pieces, then milled by wet grinding in a jar, dried, and sieved to 160 μm to obtain the CDW raw powder.

Commercial metakaolin (MK) (Argical™ M1200S, Imerys, France, SSA = 25 $m^2\ g^{-1}$, d50 = 1.5 μm) was also tested as a secondary, highly reactive precursor, in partial substitution of CDW. As alkaline activators, solutions of sodium hydroxide at different molarities (4 or 8 M) and sodium silicate solution were used. The hydroxide solutions were obtained by mixing NaOH pellets (Honeywell Fluka™, purity ≥98 %) in deionized water. Sodium silicate solution (coded NaSil) was prepared by adding 10 g of NaOH pellets dissolved in 10 g H_2O, to 100 g of commercial sodium polysilicate (Ingessil srl, Italy, modulus SiO_2:Na_2O=3.2, H_2O= 64 wt%), to obtain a final modulus SiO_2:Na_2O= 1.7 and H_2O:Na_2O=16.

2.2. Sample preparation

The slurries were prepared by mixing the CDW powder and/or the MK with the alkaline activator at room temperature using a shear mixer (Thinky Mixer ARE-500, Thinky Corporation, Japan) at 1000 rpm for 2 minutes. The slurries were then cast into cylindrical silicone molds (40 mm diameter and 20 mm height), sealed and cured for 12 h at 60°C, then cured for a further 12 h at 60°C. After demolding, the specimens were kept unsealed in a controlled laboratory environment (T: 22±2°C, RH=50±5 %).

Table 1 summarizes some of the studied material formulations with sodium hydroxide and silicate solution, labeled using Wxx to indicate the wt% of the waste powder used in the formulation, Myy to indicate the wt% of MK, and N- or S-zz to indicate the wt% of alkaline activator, with N and S standing for NaOH and NaSil, respectively. A MK-based geopolymer was also prepared as benchmark material with a Si/Al ratio of 2, using MK and sodium silicate with H_2O:Na_2O=16 in a solid to liquid weight ratio S/L=0.7 (M40S60).

These formulations were derived from a preliminary screening campaign which has been carried out, in which all variables were considered and modified one at a time. In particular, the workability and

Table 1
Materials formulations and codes: Wxx indicates the wt% of CDW, Myy indicates the wt% of MK, and N- or S-zz indicate the wt% of alkaline activator, standing N and S for NaOH and NaSil, respectively.

Sample	CDW [wt %]	MK [wt %]	NaOH 4 M [wt %]	NaOH 8 M [wt %]	NaSil [wt%]	CDW/MK	S/L
W50N(8)50	50	-	-	50	-	-	1
W50N(4)50	50	-	50	-	-	-	1
W40S60	40	-	-	-	60	-	0.7
W52M8S40	52	8	-	-	40	6.5	1.5
W44M12S44	44	12	-	-	44	3.7	1.3
W30M20S50	30	20	-	-	50	1.5	1
M40S60 (benchmark)	-	40	-	-	60	-	0.7

fresh state properties of the mixtures were evaluated comparatively with reference to the benchmark mixture based solely on MK [53].

2.3. Characterization

The unsorted CDW, after milling and sieving at 160 μm, was analyzed using a field emission gun-scanning electron microscope (FE-SEM, ZEISS Sigma, Carl Zeiss Microscopy Gmbh, Germany). To determine its granulometry, the CDW raw powder was wet-sieved through a 100-μm sieve. The material retained on the sieve, larger than 100 μm, was oven-dried at 103°C and weighed, while the finer fraction was analyzed using a gravitational particle size analyzer (SediGraph III Plus 5125, Micromeritics, USA) to measure its particle size distribution (PSD).

The true density of the CDW powder and the geopolymer samples, after pulverizing them, was measured by helium picnometry (AccuPyc II 1340, Micrometrics, USA).

X-ray diffraction (XRD) analysis, using CuKα radiation (D8 Advance, Bruker, Germany) was performed, collecting patterns from 5 to 80° (step 0.02°, step time 0.5 s), to determine the main phase composition. The XRD data were processed with Profex 5.2.9 software by the Rietveld refinement kernel BGMN for a semi-quantitative mineralogical analysis (average of three refinements per XRD pattern) of the unsorted CDW and on geopolymer samples. Also, the presence of $Ca(OH)_2$ and CaO in CDW was also confirmed by a colorimetric test using a phenolphthalein solution (1 % in ethanol). The chemical composition was determined by Energy-Dispersive X-ray Fluorescence (EDXRF) (S2 PUMA, Bruker, Germany).

The bulk apparent density [UNI-EN 1015–10: 2001], water absorption [UNI-EN 12390–7: 2011], and open porosity of the geopolymer samples were determined using a hydrostatic balance. Specimens were dried until a constant weight was reached, then weighed before and after immersion in water up to complete saturation. Water uptake, density and water-filled porosity were calculated using the following formulae [54]:

$$d_B = [w_1/(w_3\text{-}w_2)] \bullet \rho_{H2O} \quad (1)$$

$$P\% = [(w_3\text{-}w_1)\ (w_3\text{-}w_2)] \times 100 \quad (2)$$

$$A\% = [(w_3\text{-}w_1)/w_1] \times 100 \quad (3)$$

where dB, P% and A% are the bulk density, percentage of open pores and water absorption respectively. w_1 is the dry weight of the specimens in air, w_3 is the weight of the fully saturated specimens in air, and w_2 is the weight of the fully saturated specimens suspended in water.

The open porosity of the materials was also measured by mercury intrusion porosimetry (MIP Pascal 140 and Pascal 240 series, Thermo Finnigan, U.S.A.) in the pore range of 0.0058–100 μm.

Optical microscopy analysis was performed on the consolidated samples (digital microscope HIROX RH-2000, Hirox, Japan). The microstructure of the obtained materials was investigated by environmental scanning electron microscopy (ESEM Quanta 200 FEI, Thermo Fisher Scientific, U.S.A.) on sputter-coated samples using carbon or gold targets.

Mechanical properties were investigated by compressive strength tests on samples aged 28 days, with dimensions of 24 mm diameter and 25 mm height, using a universal testing machine (Z050, Zwick-Roell, Germany) in control displacement mode, with a cross-head speed of 1 mm min^{-1}.

Thermal characterization was conducted in static air at a heating rate of 20 °C/min up to 1000°C. Simultaneous thermal analysis (STA 449 C Jupiter, Netzsch Geraetebau, Germany) was used in TG+DSC mode on pulverized and bulk samples. Dilatometry (differential linear dilatometer, 402CD, Netzsch Geraetebau, Germany) was performed on bars 3 mm × 3 mm × 25 mm and a heating microscope (ODP868, TA Instruments, U.S.A.) was used on pulverized samples and cubes (5 mm side) in air at a heating rate of 10 °C/min up to 1000°C.

3. Results and discussion

3.1. CDW characterization

Raw pieces of unsorted CDW and the powder obtained by wet grinding as used in the current study are shown in Fig. 1a and b, respectively.

Most of the CDW powder is finer than 100 μm, with only around 0.5 wt% of the particles falling in the range of 100–160 μm. The PSD is reported in Fig. 2. D50 was set at 3.53 μm, while D90 was 17.6 μm and D10 was 1.05 μm. The true density measured by He-pycnometer was 2.693 g·cm^{-3}.

The X-ray diffractogram is reported in Fig. 3, where the main peak assignments are shown. Sharp peaks clearly indicate the presence of crystalline minerals. The unsorted CDW powder is mainly composed of quartz (SiO_2), identified as the major constituent, calcite ($CaCO_3$), and feldspars. The latter, in particular, are present mainly as K-feldspar such as microcline and orthoclase ($KAlSi_3O_8$), albite ($NaAlSi_3O_8$), and anorthite species ($CaAl_2Si_2O_8$), while anorthoclase ($Na,K)AlSi_3O_8$), sanidine ($(K,Na)AlSi_3O_8$) and andesine ($(Ca,Na)(Al,Si)_4O_8$) were identified as minor phases. The presence of other silicate minerals in trace amounts was also identified, among these were phyllosilicate mineral of aluminum and potassium e.g., muscovite polytypes ($KAl_2Si_3AlO_{10}(OH)_2$ and $(K,Na)(Mg,Fe)_2(Si_{3.1}Al_{0.9})O_{10}(OH)_2$), enstatite ($MgSiO_3$-(Mg,Fe)$SiO_3$) in the pyroxene group, as well as gismondine ($CaAl_2Si_2O_8 \bullet 4\ H_2O$) and chlorite group minerals in very low concentrations.

XRD analysis also revealed phases typically present in building materials, as calcium sulfate hemihydrate (bassanite, $CaSO_4 \cdot 0.5\ H_2O$) and traces of anhydrite ($CaSO_4$) and gypsum $CaSO_4 \cdot 2\ H_2O$). A broad hump centered around 2θ=29–32° is attributable to amorphous to semi-crystalline calcium silicate hydrates (C-S-H), which are the primary products of the hydration of Portland cement. Additionally, other crystalline phases typically of hydrated cement as portlandite ($Ca(OH)_2$) were not found neither by XRD analysis nor by phenolphthalein test, showing no change in color on the surface of different demolition waste materials (including cement mortar) as well as on powder after milling. This suggested that all free lime eventually present in the waste building material underwent complete carbonation over the years by reacting with atmospheric CO_2.

The semi-quantitative XRD analysis (Table 2), although it did not highlight the presence of reactive hydraulic phases as calcium silicates, pointed out the presence of relatively unstable phases, such as calcium sulfates (8 %), whose behavior in the presence of aqueous and alkaline solutions might affect the reaction mechanisms in the alkaline environment of the geopolymer [55,56]. Conversely, detected Si-Al rich feldspars and alkaline earth carbonates could partially act as geopolymer precursors or inert phases, respectively, especially in highly alkaline environments [57–59].

The chemical composition for CDW powder obtained by XRF is

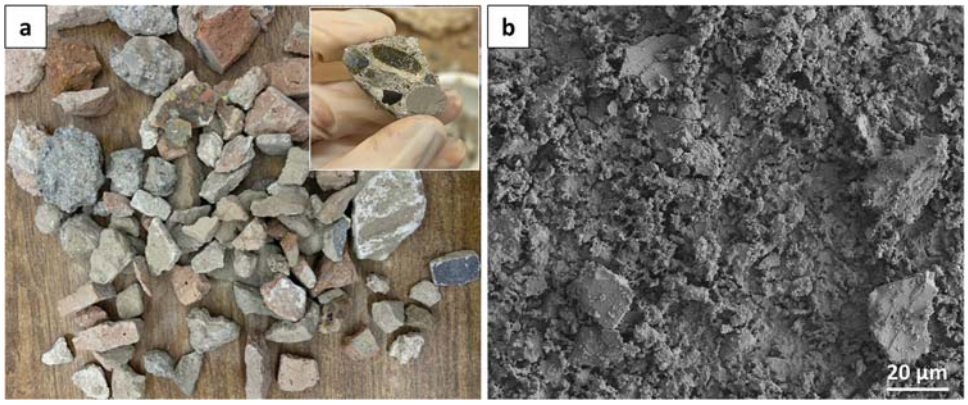

Fig. 1. Unsorted CDW from a demolished residential building, containing brick, cement mortar and natural stone scraps (a) and SEM micrograph of the milled and sieved powder (b).

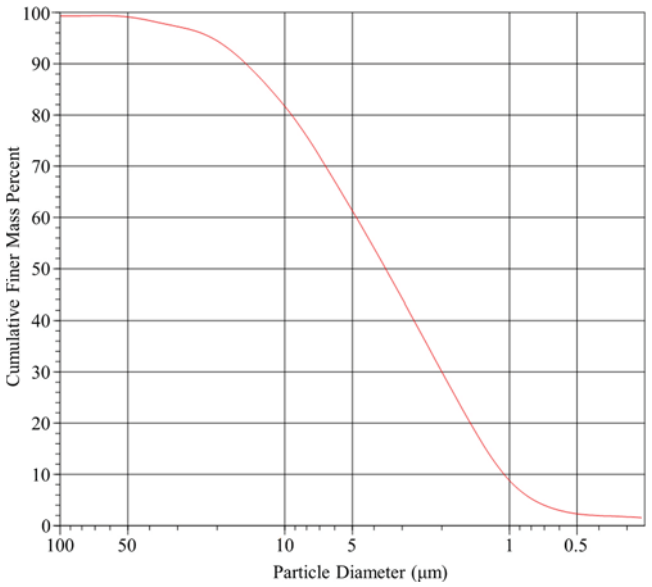

Fig. 2. PSD of the unsorted CDW powder (100–160 μm fraction) obtained by milling and sieving at 160 μm.

reported in Table 3, which is basically consistent with the mineralogical and semi-quantitative analyses. The CDW primarily consists of SiO_2 (~47 %), along with a notable presence of CaO (~19 %) and Al_2O_3 (~10 %), and minor amounts of the other major constituents. Such composition reflects the use of mixed construction and demolition waste, with a high proportion of masonry and ceramic materials containing aluminosilicates species. The relatively high content of CaO could be attributed primarily to the presence of carbonate-rich clays, in agreement with the estimated amount of calcium carbonates around 17 % (Table 2), but also to aged cement mortar.

3.2. Synthesis of CDW-based geopolymer

Based on its mineralogical characterization the most suitable reactive systems for CDW consolidation have been explored moving from NaOH solutions with decreasing concentration (8 and 4 M), commercial Na polysilicate solution, to mixed solutions of alkali hydroxide and silicate (namely sodium silicate solution, NaSil) (Table 1). First attempts to use Na polysilicate alone caused undesirable flash setting phenomena likely due to a pozzolanic reaction occurring between the silicates of the solution and calcium hydroxide [60], in turn deriving from available Ca^{2+} ions from the dissolution of bassanite in the reaction medium [56, 61]: this resulted in unevenly agglomerated materials, only partially consolidated (data not reported).

The formation of alkaline carbonates (efflorescences) was found on hardened materials formed by using hydroxide solutions independently of the molarity and was caused by the presence of an excess of free alkalis in the system (Fig. 4a). In turn, good compatibility of the waste powder was observed with aqueous activator based on sodium silicate (Fig. 4b). In fact, such mixed activator simultaneously allowed to limit or avoid the drawbacks related to the single use of silicates or hydroxide solutions. Unfortunately, even if the structure was apparently good (Fig. 4b), the samples were brittle for handling, indicating the need for a more effective process of material consolidation.

The mixtures formulated by adding MK in partial replacement of CDW, improved geopolymerization and the homogeneity of the microstructure. Fig. 5 shows the images of samples obtained using the mixed activator varying the CDW/MK ratio from 6.5 to 1.5 in order to optimize the consolidation. The best result was obtained with CDW/MK ratio equal to 1.5. In that case the macropores due to air entrapment formation were limited, unlike to the case of higher CDW amounts and the cohesion was good enough to justify no further increase of MK amount. Furthermore, the solid/liquid weight ratio (S/L) varied from 0.7 to 1.5 in function of the workability of the slurries due to the different densities of the alkaline solutions (namely 1.15 g/ml for NaOH 4 M, 1.28 g/ml for NaOH 8 M and 1.50 g/ml for NaSil), as well as the reactivity of the powders. The addition of a small amount of MK allowed a good homogenization of the slurries and setting of the samples using higher S/L ratios than when CDW powder was used alone (Table 1). However, the amount of liquid phase needed to be increased again when increasing the amount of MK due to its high specific surface and reactivity [57].

3.3. Microstructural, textural and mechanical characterization of the CDW-based geopolymers

Fig. 6 shows the digital optical microscope images of bottom surfaces in contact with the mold of W40S60 and W30M20S50: it is evident that a high quantity of unreacted NaSil is present in the former, while a homogeneous surface with finely subdivided precipitates is visible in the latter. SEM images in Fig. 7 show the microstructure of the fracture surfaces after 28 days of aging. W50N(8)50 (Fig. 7a) had smooth areas covered by a glassy phase formed due to leaching caused by the high alkalinity of NaOH. In fact this feature almost disappeared in W50N(4)50 (Fig. 7b). As for W40S60 (Fig. 7c), thick intergranular cracks occurred along the edges of the unreacted CDW particles and within the matrix which appeared denser than a typical MK-based geopolymer due to the unreacted silicate (Fig. 6a). Concerning samples with the addition of MK, while the microstructure appeared porous and incoherent in W52M8S40 (Fig. 7d) with low amounts of MK and NaSil, in

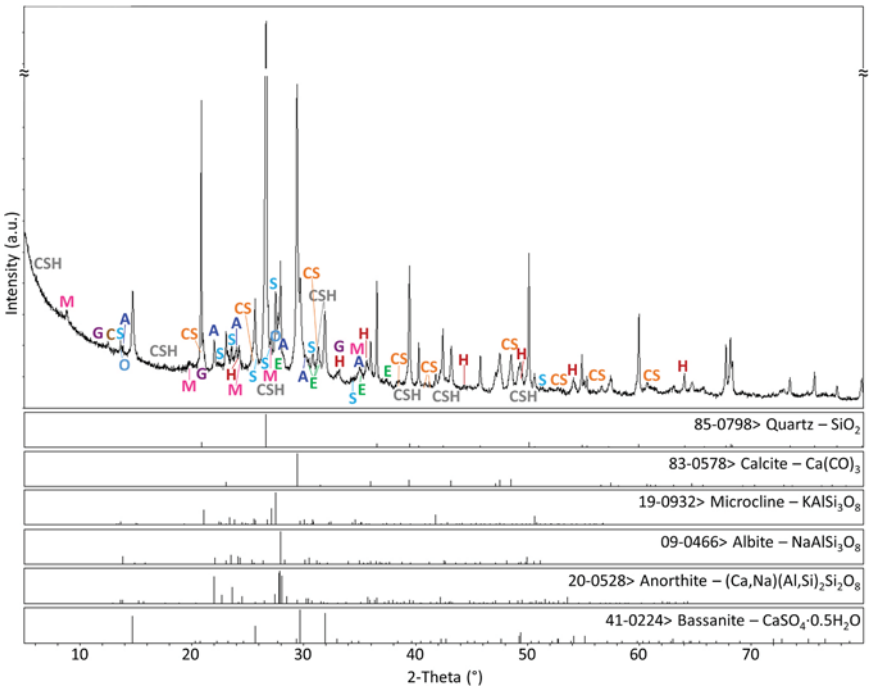

Fig. 3. XRD pattern of unsorted CDW powder. At the bottom, the heights and positions of the peaks for the main mineralogical phases. Minor and traces phases are indicated as: CS: calcium sulfate phases, such as anhydrite and gypsum; S: sanidine; A: andesine; O: anorthoclase; M: muscovite; E: enstatite; H: hematite; CSH: calcium silicate hydrate, G: gismondine; C: chlorite group minerals.

Table 2
Semi-quantitative analysis of unsorted CDW powder.

Mineralogic composition [wt%] (±2 %)	
Quartz	28
Feldspars	33
Phyllosilicates	4
Carbonates	17
C-S-H (Ca silicates hydrates)	8
Ca Sulphates	8
Others	2

W44M12S44 (Fig. 7e) cracks appeared in the glassy matrix due to a higher amount of silicate in the formulation. Finally, W30M20S50 (Fig. 7f) presented a fine microstructure as observed macroscopically in Fig. 6b and no evidence of unreacted silicates was found.

Table 4 reports true densities by He-pycnometer, bulk apparent densities, total porosities and water adsorption measured by the Archimedean method and data resulted from MIP analysis of samples prepared using NaSil solution. Archimedean total porosity was a few percentage points higher than the open porosity measured by MIP due to the presence of pores outside the MIP range, mainly over 100 μm. As expected, this difference increased when glassy phase was detected as in the case of W40S60 (Figs. 6a, 7c) and W44M12S44 (Fig. 7e) due to the sealing of small pores, while the water absorption increased congruently with the open porosity. The most interesting data are related to pore size distribution that showed the presence of mesoporosity (Fig. 8). In detail, besides the low porosity W40S60 had a modal pore size of 0.031 μm (Fig. 8a) and W44M12S44 of 0.029 μm (Fig. 8c). W30M20S50 had a monomodal distribution with modal pore size of 0.021 μm (Fig. 8d) as the benchmark MK-based geopolymer with modal pore size of 0.022 μm (Fig. 8e), while the MIP open porosities differed by being 42 % in the former and 36 % in the latter because of the different amount of water in the starting formulation [62]. Concerning W52M8S40 (Fig. 8b), the modal pore size of 0.6682 μm again aligned with the porous and incoherent appearance of Fig. 7d, making clear that such formulation had a content of silicate activating solution too low to promote the formation of a geopolymer binder.

W30M20S50 was selected for further analyses due to the microstructural and porosimetric features resembling a MK-based geopolymer, despite as much as 60 % of the aluminosilicate powder being made up of CDW. In particular, the compressive strength of W30M20S50 after 28 days was 25 ±2 MPa, in agreement with MK-based geopolymer having the same type of porosity (27 ±5 MPa) [63], although the obtained values may be slightly overestimated (about 15 %) due to the low slenderness of the tested samples [64].

The pore content and the pore distribution determine both the capillary suction capacity and the mechanical characteristics of the material and therefore can determine their most suitable application conditions. In particular, the remarkable presence of pores < 0.1μm, might ensure high breathability and very low capillary absorption, making such formulation suitable for applications as indoor partitions, vapor permeable mortars and plasters in eco-building construction and restoration [65,66].

3.4. Thermal behavior

In Fig. 9 the comparison of the TG-DSC curve of CDW raw powder

Table 3
Chemical composition of the unsorted CDW powder. * BaO, ZnO, Cr_2O_3, SrO, Sb_2O_3.

	Oxides, Mass percentage (wt%)											Loss on Ignition LOI
	SiO_2	Al_2O_3	Fe_2O_3	CaO	MgO	K_2O	Na_2O	TiO_2	P_2O_5	MnO	Traces*	
CDW	47.57	10.29	3.54	19.03	1.53	1.78	1.36	0.37	0.35	0.14	0.15	13.90

Fig. 4. Images of samples (diameter 40 mm, height 20 mm) W50N(8)50 (a), W40S60 (b).

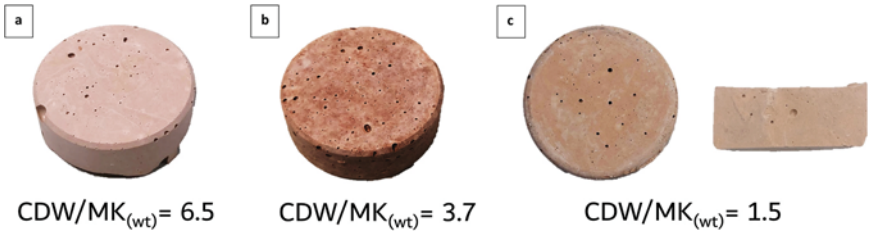

Fig. 5. Images of samples (diameter 40 mm, height 20 mm) W52M8S40 (a), W44M12S44 (b) and W30M20S50 (c) obtained using the mixed activator and varying the CDW/MK ratio.

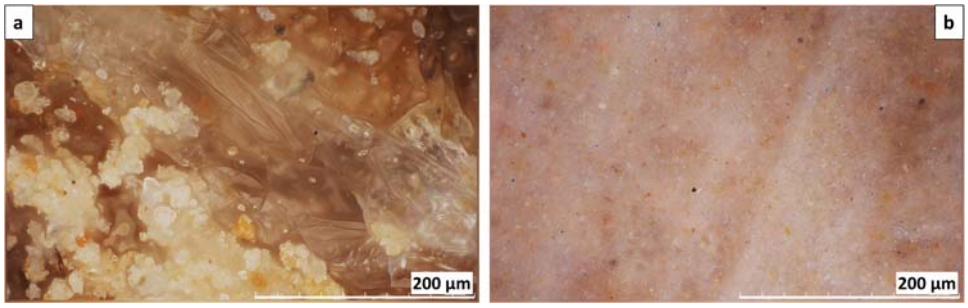

Fig. 6. Digital optical microscopy of bottom surfaces in contact with the mold of W40S60 (a) and W30M20S50 (b).

and of W30M20S50 is shown. A first small weight loss occurred in the temperature range from 20°C to 220°C due to the dehydration and the removal of structural water from the different phases constituting the materials. As for CDW powder, the dehydration is mainly related to the loss of physically bound water from C-S-H phases and Ca-sulphates. Similarly, the weight loss of W30M20S50 in this temperature range is related to the thermal behavior of the geopolymer phases, linked with the moisture loss and elimination of free water from the pores of the material and to structural water typical of some phases. A second mass loss event (about 8.3 wt%) due to CO_2 emission linked to decarbonation phenomena is detected in W30M20S50 in the range of 600–900°C, which allows to estimate the carbonates content in the CDW as 19 wt%, in good agreement with the value found from XRD semiquantitative analysis (17 %). The thermal decomposition of carbonates, both for CDW powder and for the geopolymer sample, is also detectable by observing the two endothermic peaks in the DSC curve, located around 600°C and 800°C respectively. These peaks include also, to a lesser extent, the endothermic signal due to the complete decomposition of the C-S-H structures into anhydrous phases (wollastonite). Comparing the curves of the CDW raw powder and W30M20S50, the estimated CDW content in the CDW-based geopolymer is equal to 39 % by weight, in agreement with that present in W30M20S50 after consolidation. Such good agreement indicates the presence of very little unreacted alkali NaSil, that could have converted later into carbonated phases contributing to decarbonation.

Dilatometric and derivative curves of W30M20S50 and benchmark MK-based geopolymer M40S60 are compared up to 1000°C in Fig. 10a. In agreement with literature [67–69], as the temperature increases in the range of 20–700° C, the dilatometric thermal profile of W30M20S50 can be divided into four regions, each reflecting different thermal events. After maintaining dimensional stability up to above 150°C (I region), a first rapid shrinkage with an onset temperature of 156°C was detected (II region), which is attributable to dehydration. Those phenomena include the loss of residual and pore-trapped water and are highlighted by the negative peaks in the derivative curves. At about 250°C thermal shrinkage slowed down in relation to dehydroxylation of

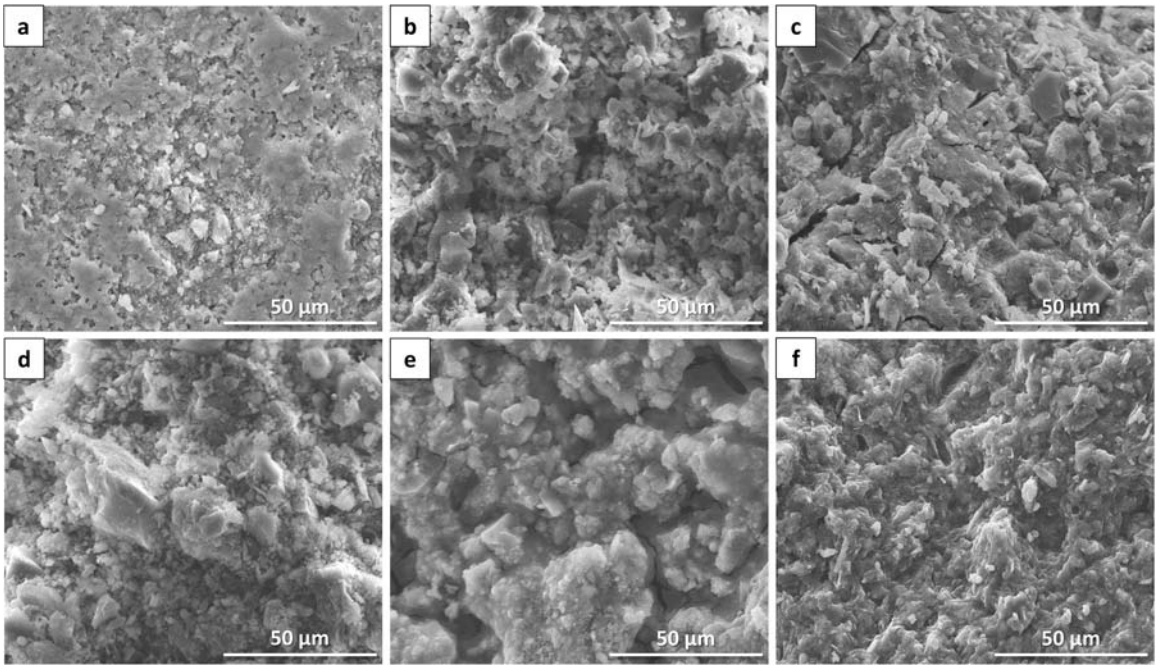

Fig. 7. ESEM micrographs of fracture surfaces of W50N(8)50 (a), W50N(4)50 (b), W40S60 (c), W52M8S40 (d), W44M12S44 (e) and W30M20S50 (f) after 28 days of aging.

Table 4
True densities by He pycnometry, bulk apparent densities, total porosities and water adsorption measured by the Archimedean method and data resulted from MIP analysis in the range 0.0058–100 microns of samples prepared using sodium silicate solution.

Sample	True density [g/cm^3]	Bulk apparent density [g/cm^3]	Total porosity [%]	Water absorption [%]	MIP Bulk density [g/cm^3]	MIP open porosity [%]	Total intruded V [mm^3/g]	Median pore d [µm]	Modal pore d [µm]
W40S60	2.478 ± 0.002	1.87 ± 0.01	25	6.7 ± 0.2	1.86	20	106.9	0.0335	0.0310
W52M8S40	2.527 ± 0.004	1.22 ± 0.02	53	28.0 ± 0.8	1.21	50	415.2	0.5769	0.6682
W44M12S44	2.476 ± 0.006	1.35 ± 0.06	45	22.0 ± 1.5	1.46	41	278.7	0.0334	0.0291
W30M20S50	2.428 ± 0.006	1.35 ± 0.02	44	21.3 ± 0.2	1.36	42	305.6	0.0233	0.0214

aluminate and silicate groups (T-OH, T= Si, Al) (III region). Over 600°C (onset temperature at 648°C) a second rapid shrinkage took place due to the material densification by viscous flow (IV region). Unlike the benchmark (Fig. 10a) and typical MK-based geopolymer [67–69], a quick expansion started at 739°C followed by a slight shrinkage and a plateau over 800°C, suggesting that the densification process also caused relevant dimensional instability in the material. In fact, the CDW-MK geopolymer specimen was partially fractured on the surface and microcracks were detected, owing to thermal stresses and recrystallization. Indeed, while typical crystallization in MK-based geopolymers occurs at higher temperatures (Fig. 10a), it is feasible for certain crystalline phases (nepheline, anorthite), to begin forming over 700°C in a unsorted CDW-derived geopolymer, especially in the presence of alkali metals and calcium. The same thermal behavior was observed in W30M20S50 with the heating microscope (Fig. 10b), whereas the expansion was not seen in the sample prepared by pressing the powder after crushing W30M20S50, due to the ability of the loose powder to dissipate deformation stresses and facilitate any gas escape without generating fractures in the material.

Fig. 11 compares the microstructure of the benchmark and W30M20S50 before and after dilatometric test at 1000°C. The homogeneous and fine-grained microstructure of the benchmark (Fig. 11a) became compact and smooth due to glass formation and the conversion into nepheline (Fig. 11c) [61], while the rounded pores caused by air entrapped during consolidation were still evident. In contrast, W30M20S50 which was predominantly homogeneous (Fig. 7f), but with some local inhomogeneity due to large CDW particles and traces of unreacted silicate (Fig. 11b), after thermal test assumed a "foamed" structure. Comparing the porosimetric distribution of W30M20S50 before (Fig. 8e) and after (Fig. 8f) the thermal tests, the shift of the porosity is evident from the mesopore to the macropore range with a modal pore diameter equal to 3.723 µm (Fig. 8f) and a total porosity as measured by MIP of 25 %. SEM analysis also revealed the formation of ultra-macropores beyond the MIP detection range, showing both large rounded-shaped pores with diameter up to ~160 µm and irregularly shaped pores due to coalescence of smaller jagged pores in the foam structure (Fig. 11d). However, the density increased (1.43 g/cm^3) due to initial shrinkage.

Fig. 12 shows X-ray diffraction patterns of the CDW-based geopolymer W30M20S50 before and after dilatometric test. The sample before dilatometric test clearly shows evidence of newly formed amorphous species, as suggested by the broad hump in the region from 20 to 35 2θ, which can be related to the formation of geopolymer phases mainly from metakaolin. Most of the minerals observed in the raw CDW powder are identified also in the geopolymer material, such as quartz, alkali feldspars (i.e. microcline) and plagioclase feldspars (i.e. albite,

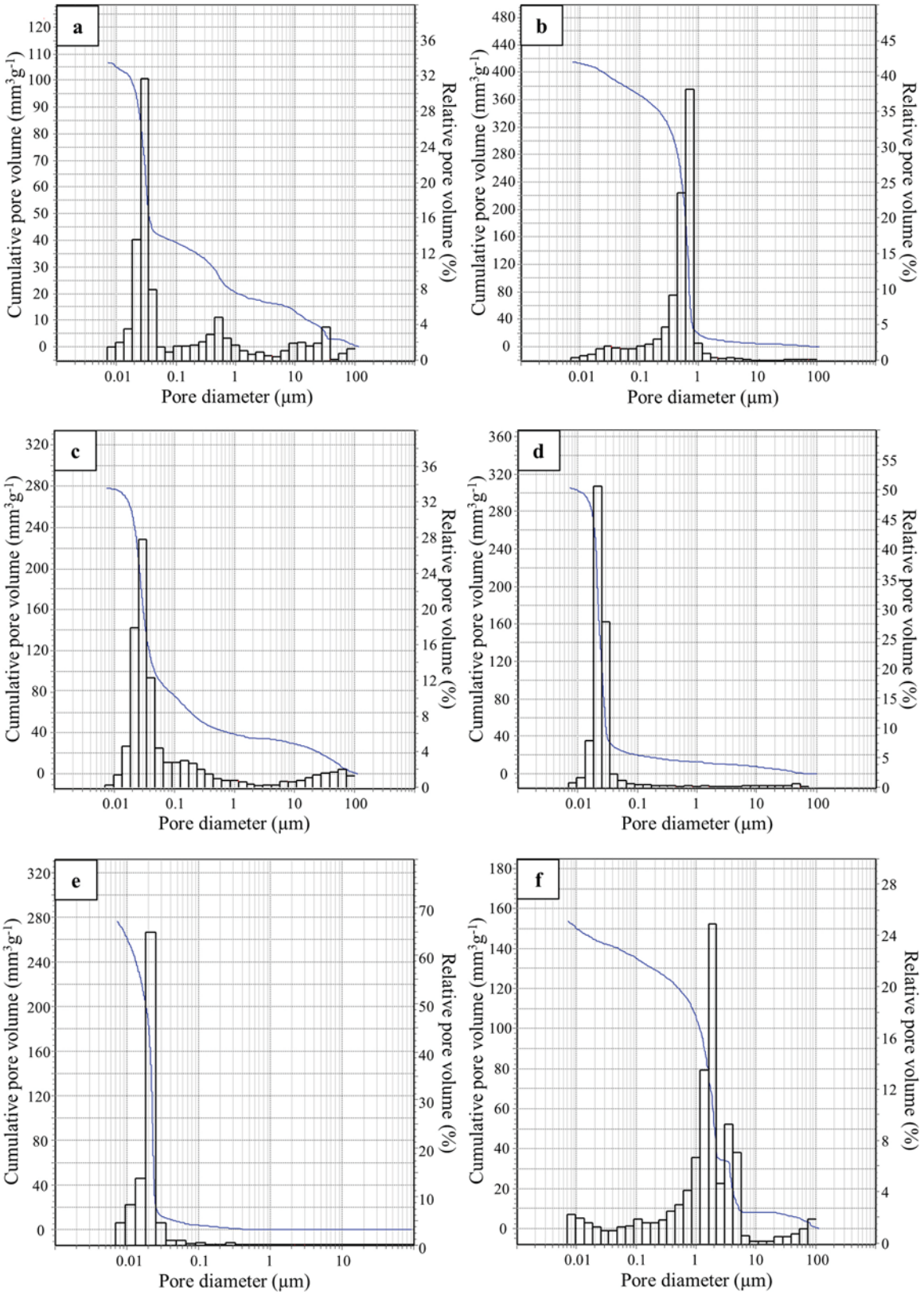

Fig. 8. Pore size distribution of W40S60 (a), W52M8S40 (b) W44M12S44 (c), W30M20S50 (d), the benchmark MK-based geopolymer M40S60 (e) and W30M20S50 after dilatometric analysis at 1000°C (f).

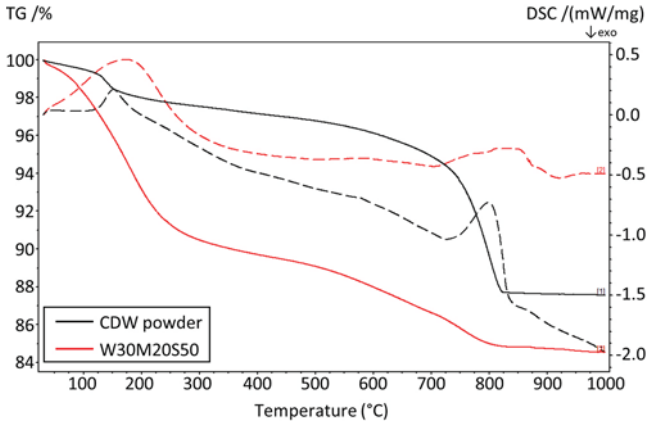

Fig. 9. TG (solid lines) and DSC (dashed lines) curves for CDW powder and W30M20S50 sample.

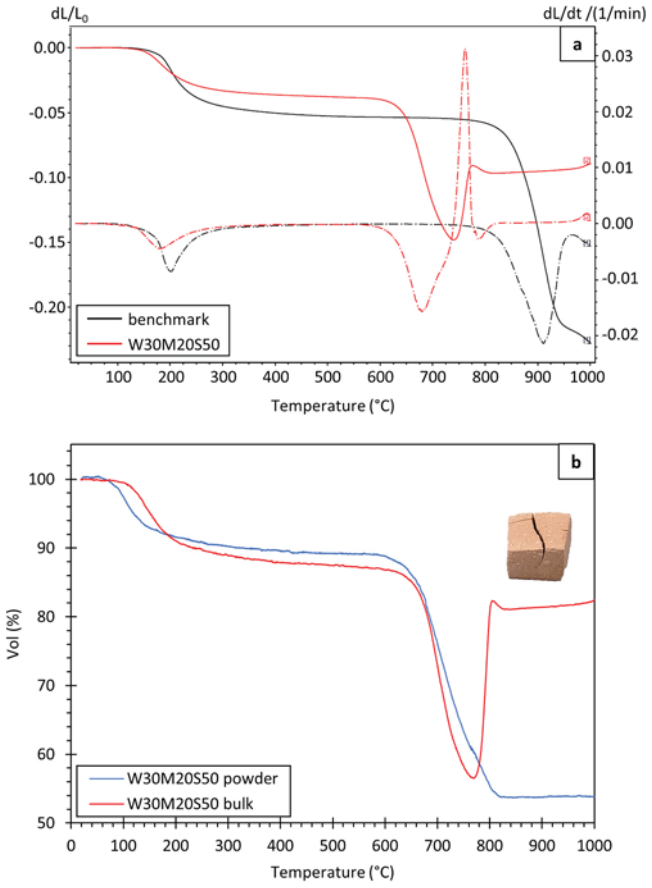

Fig. 10. Dilatometric (solid lines) and derivative (dashed) curves of benchmark MK-based geopolymer M40S60 and sample W30M20S50 (a), and heating microscope curve of W30M20S50 and its pressed powder (b). In the box the cubic sample W30M20S50 after the test.

anorthite, sanidine, etc.). Their prominent peaks could suggest a reduced involvement in the polycondensation reactions. Nevertheless, a partial dissolution of some of the aluminosilicates from the CDWs in the geopolymer matrix is also plausible, given the high alkalinity of the environment. In fact, Ca ions dissolved in the system could have nucleated amorphous C-(A)-S-H phases rather than C-S-H. The formation of the C-(A)-S-H within environments at high pH is in accordance with previous literature data on alkali activation of high Ca-containing precursors [70]. Similarly, the peak intensities of gismondine ($CaAl_2Si_2O_8{\cdot}4\ H_2O$), which was found in traces in the CDW precursor, did not decrease or disappeare: this high calcium-containing zeolite type gel has previously been reported as the main reaction product in alkali activated slag [71].

With respect to the raw CDW powder (Fig. 3), the consolidated material shows no peaks for bassanite or other hydrated calcium sulphates, while sodium sulphate was detected in traces, confirming the plausibility of the formation of portlandite ($Ca(OH)_2$) along with thenardite (Na_2SO_4) from the decomposition of the calcium sulphates in the presence of high concentrations of free OH^- in the system [61]. The absence of $Ca(OH)_2$ in the spectrum is due to its complete carbonation, as also revealed by the peaks of $CaCO_3$ detected in the diffractogram, owing to a prolonged exposure of the sample before the XRD analysis.

The sample after dilatometric test up to 1000°C, compared to the specimen before test, resulted in a reduction of the amount of amorphous phase, as noted by the lowering of the hump, and in the conversion of the amorphous geopolymeric phases into thermally stable crystalline phases, such as nepheline ($(Na, K)AlSiO_4$), which appears as the major phase in the thermally treated CDW. Along with the crystallization of the geopolymer-derived alkali aluminosilicate network, the transition of CDW-derived C-S-H and other Ca-bearing silicates into wollastonite ($CaSiO_3$) was also observed. As well as the partial conversion of quartz (SiO_2) and orthoclase ($KAlSi_3O_8$) into their high temperature polymorphs, tridymite and sanidine, respectively. Secondary phases mainly include Na-rich anorthite ($(Ca, Na)(Si, Al)_4O_8$) and kyanite (Al_2SiO_5).

Therefore, from the analysis it could be hypothesized that the expansion starting from around 740°C could be due to the presence of carbonates ($CaCO_3$), which by developing gas unable to escape from the viscous system cause an expansion of the sample and the formation of pores as in Fig. 11d. Furthermore, the expansion could also be due to the presence, even if minor, of phases such as pyroxenes (enstatite present in CDW, Fig. 3), which undergo reduction, thus releasing O_2, which produces bubbles in the viscous mass of the sample. Generally, the viscosity of the system decreases as the temperature increases, and a small shrinkage is observed at around 780°C. The expansion phenomenon counterbalances the shrinking trend of the material itself (powdered sample, Fig. 10b), so that at this temperature a small shrinkage is detected in the bulk specimen, as a completion of the contraction. Afterwards, the system expands again, albeit in a limited manner due to crystallization. The crystallization and allotropic transformations are evidenced by the DSC signals detected at high temperature, when TG curve is constant (Fig. 9). Furthermore, the mismatch between the thermal expansion coefficients of the geopolymer-derived phases (nepheline) and of those deriving from re-crystallization of Ca-rich phases in CDW (wollastonite) also favors the formation of porosity in the sample [72].

The fracture of W30M20S50 after thermal test can be ascribed to different factors previously discussed, such as local microstructural inhomogeneities (Fig. 11 b), the formation of entrapped gas (which in the case of the pressed powder sample can easily escape from the specimen without leading to expansion), and the mismatch in the thermal expansion coefficients of newly formed crystalline phases.

4. Conclusions

This paper investigated the potential of unsorted CDW collected from a residential building as a precursor to produce AAMs/ geopolymers.

- While CDW exhibited low to medium reactivity in an alkaline environment for the relevant presence of inert mineral phases, a proper geopolymer-like material was obtained by using MK in partial substitution of CDW and using aqueous activators based on jointly mixed Na-silicates and hydroxides.
- A well reacted and cohesive material was obtained with a MK/CDW weight ratio of 40/60, which showed an open porosity ~42 % with a

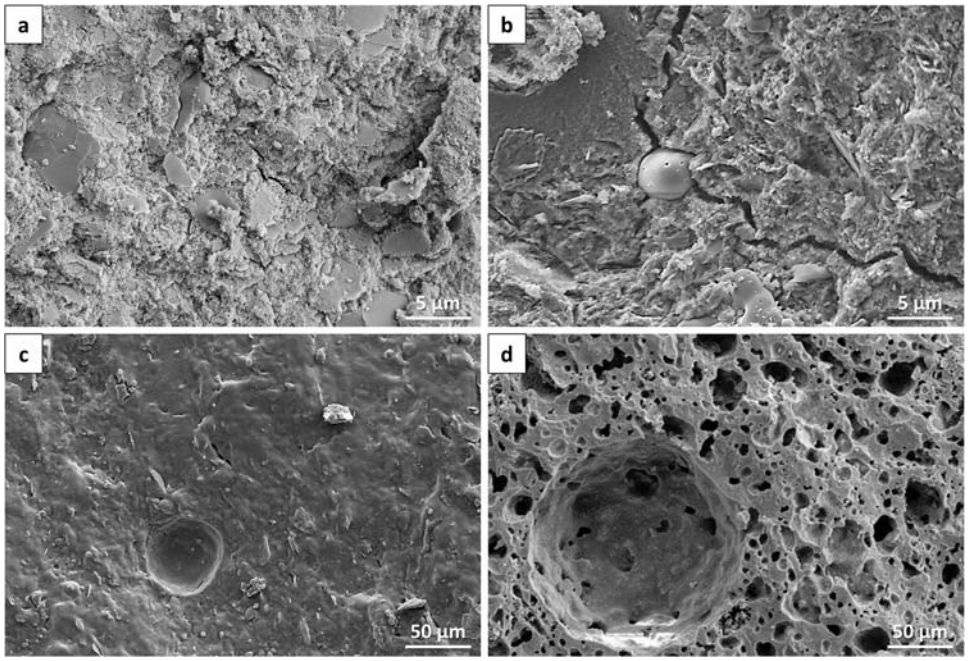

Fig. 11. SEM micrographs of benchmark MK-based geopolymer M40S60 (a, c) and W30M20S50 (b, d) before (a, b) and after (c, d) dilatometric test.

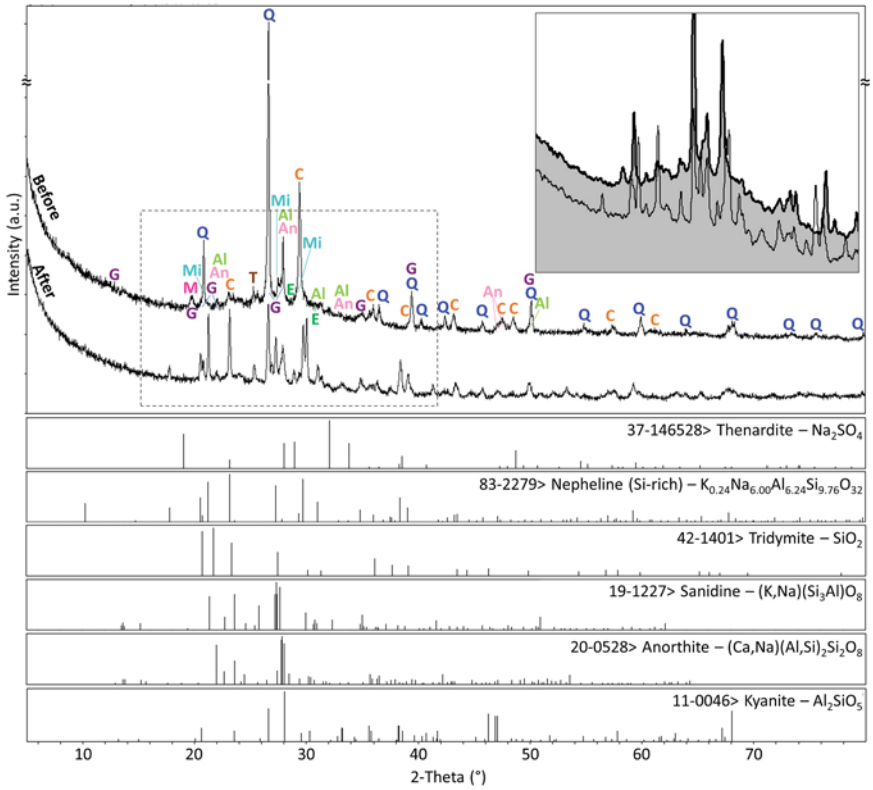

Fig. 12. XRD patterns of W30M20S50 sample before and after dilatometric test in air up to 1000°C. In the inset, magnification image of patterns in the dotted line box highlighting amorphous humps. At the bottom, the heights and positions of the peaks for the main phases due to geopolymerization and heating to 1000°C. The mineralogical phases sourced from CDW (Q: quartz; C: calcite; Mi: microcline; Al: albite; An: anorthite; M: muscovite; G: gismondine; E: enstatite) and MK (T: titanium oxide) are displayed on the pattern.

monomodal distribution, typical for solid geopolymer materials, and a 28dd compressive strength of 25 ±2 MPa, in line with MK-based geopolymers having the same porosity (27 ±5 MPa).

- The formulated CDW/MK-based geopolymer remained thermally stable up to 650°C, although beyond this temperature shrinkage due to viscous flow was observed, followed by expansion above 750°C, likely due to the formation of gases trapped in the matrix and the differing thermal expansion rates of new crystalline phases. At temperatures up to 1000°C, microstructural analysis revealed the development of dense struts and macropores, while the open

porosity decreased to 25 % due to sintering in the geopolymeric matrix.

In summary, the mechanical and thermal results highlighted a good potential for CDW-based geopolymers for uses in green building applications, with good thermal stability up to medium-high temperatures. The high porosity and small pore sizes of the material also suggest good thermal and acoustic insulation properties, making it suitable for use in insulation panels or as a component in green insulation systems. Also, the mechanical strength of 25 MPa is adequate for non-structural applications such as plaster, fillers, or lightweight blocks. Its breathability (high porosity and small pores) makes it suitable for use in historic building materials or restorations, where it is important for the material not to trap moisture, thus preventing damage to existing structures. This, in conjunction with the reuse of earth-abundant waste, low processing technologies and reduced CO_2 emission when compared to traditional cements, makes this kind of material very attractive. Moreover, since very little information concerning the thermal behavior of this kind of material has been given in literature, the spontaneous formation of foam-like porous structure above 700°C is of great interest for further investigations, in view of applications for example as insulators and lightweight panels.

CRediT authorship contribution statement

Elena Landi: Writing – review & editing, Supervision, Formal analysis, Data curation, Conceptualization. **Valentina Medri:** Writing – review & editing, Writing – original draft, Validation, Supervision, Methodology, Data curation, Conceptualization. **Elettra Papa:** Investigation, Formal analysis, Data curation. **Annalisa Natali Murri:** Writing – review & editing, Writing – original draft, Formal analysis, Data curation, Conceptualization. **Francesca Servadei:** Writing – original draft, Methodology, Investigation, Formal analysis, Data curation.

Declaration of Competing Interest

The authors declare that they have no known competing financial interests or personal relationships that could have appeared to influence the work reported in this paper.

Acknowledgements

Thanks are due to the "Circular and Sustainable Made in Italy Extended Partnership (MICS)" funded by the European Union Next-Generation EU (Piano Nazionale di Ripresa e Resilienza (PNRR) - Missione 4, Componente 2, Investimento 1.3 - D.D. 1551.11-10-2022, PE00000004) for financial support. This manuscript reflects only the authors' views and opinions, neither the European Union nor the European Commission can be considered responsible for them.

Authors also acknowledge the Emilia-Romagna Region for financial support through the project "ReWINDS - Recycling of Waste Into New Demonstrated Sustainable Solutions" (funded under the call of the Emilia-Romagna ERDF Regional Program 2021-2027, Action 1.1.2 - CUP: E27G22000290007, PG/2023/311857).

The authors warmly thank Guia Guarini for granulometric and optical dilatometry analyses, Andreana Piancastelli for XRD analysis, Dr. Sabrina Gualtieri and Dr. Sonia Conte for XRF analysis, Cesare Melandri for digital microscopy analysis and mechanical tests, and Mariachiara Gaspari for her valuable help in materials processing.

Data availability

Data will be made available on request.

References

[1] Construction and demolition waste - European Commission, (n.d.). ⟨https://environment.ec.europa.eu/topics/waste-and-recycling/construction-and-demolition-waste_en⟩ (accessed June 4, 2024).
[2] J. Soto-Paz, O. Arroyo, L.E. Torres-Guevara, B.A. Parra-Orobio, M. Casallas-Ojeda, The circular economy in the construction and demolition waste management: a comparative analysis in emerging and developed countries, J. Build. Eng. 78 (2023) 107724, https://doi.org/10.1016/j.jobe.2023.107724.
[3] G.J. Cristobal, D. Caro, G. Foster, G. Pristera, F. Gallo, D. Tonini, Techno-economic and environmental assessment of construction and demolition waste management in the European Union, Publications Office of the European Union, 2024, https://doi.org/10.2760/721895.
[4] L.A. López Ruiz, X. Roca Ramón, S. Gassó Domingo, The circular economy in the construction and demolition waste sector – a review and an integrative model approach, J. Clean. Prod. 248 (2020) 119238, https://doi.org/10.1016/j.jclepro.2019.119238.
[5] M. Bravo, J. de Brito, J. Pontes, L. Evangelista, Durability performance of concrete with recycled aggregates from construction and demolition waste plants, Constr. Build. Mater. 77 (2015) 357–369, https://doi.org/10.1016/j.conbuildmat.2014.12.103.
[6] P. Plaza, I.F. Sáez del Bosque, M. Frías, M.I. Sánchez de Rojas, C. Medina, Use of recycled coarse and fine aggregates in structural eco-concretes. Physical and mechanical properties and CO_2 emissions, Constr. Build. Mater. 285 (2021) 122926, https://doi.org/10.1016/j.conbuildmat.2021.122926.
[7] F.A.H. Saleh, N. Leklou, K. Ayed, Physico-mechanical and thermal properties of vibrating and self-compacting sand concrete based on recycled aggregate from concrete, Constr. Build. Mater. 429 (2024) 136321, https://doi.org/10.1016/j.conbuildmat.2024.136321.
[8] L. Wu, Z. Sun, Y. Cao, Modification of recycled aggregate and conservation and application of recycled aggregate concrete: a review, Constr. Build. Mater. 431 (2024) 136567, https://doi.org/10.1016/j.conbuildmat.2024.136567.
[9] V. Revilla-Cuesta, F. Fiol, P. Perumal, V. Ortega-López, J.M. Manso, Using recycled aggregate concrete at a precast-concrete plant: a multi-criteria company-oriented feasibility study, J. Clean. Prod. 373 (2022) 133873, https://doi.org/10.1016/j.jclepro.2022.133873.
[10] R. Minunno, T. O'Grady, G.M. Morrison, R.L. Gruner, M. Colling, Strategies for applying the circular economy to prefabricated buildings, Buildings 8 (2018) 125, https://doi.org/10.3390/buildings8090125.
[11] Z. Liu, L. Sun, J. Zhai, W. Huang, A review of design methods for cold in-place recycling asphalt mixtures: design processes, key parameters, and evaluation, J. Clean. Prod. 370 (2022) 133530, https://doi.org/10.1016/j.jclepro.2022.133530.
[12] Y. Xue, C. Liu, Q. Shi, Z. Ju, G. Fan, C. Zhang, S. Lv, Road performance and mechanism of Hot in-place recycling asphalt mixture modified by direct-to-plant SBS, Constr. Build. Mater. 416 (2024) 135122, https://doi.org/10.1016/j.conbuildmat.2024.135122.
[13] S. Shooshtarian, T. Maqsood, P.S.P. Wong, M. Khalfan, R.J. Yang, Review of energy recovery from construction and demolition waste in Australia, J. Constr. Eng. Manag. Innov. 2 (2019) 112–130, https://doi.org/10.31462/jcemi.2019.03112130.
[14] B. Shamurad, N. Gray, E. Petropoulos, S. Tabraiz, K. Acharya, M. Quintela-Baluja, P. Sallis, Co-digestion of organic and mineral wastes for enhanced biogas production: reactor performance and evolution of microbial community and function, Waste Manag 87 (2019) 313–325, https://doi.org/10.1016/j.wasman.2019.02.021.
[15] M.J. Whittaker, K. Grigoriadis, M. Soutsos, W. Sha, A. Klinge, S. Paganoni, M. Casado, L. Brander, M. Mousavi, M. Scullin, R. Correia, T. Zerbi, G. Staiano, I. Merli, I. Ingrosso, A. Attanasio, A. Largo, Novel construction and demolition waste (CDW) treatment and uses to maximize reuse and recycling, Adv. Build. Energy Res. 15 (2021) 253–269, https://doi.org/10.1080/17512549.2019.1702586.
[16] J. Davidovits, Geopolymer Cement a review, Geopolymer Sci. Tech. Technical Paper #21 (2013). Geopolymer Institute Library, ⟨www.geopolymer.org⟩ (accessed June 6, 2024).
[17] N.B. Singh, B. Middendorf, Geopolymers as an alternative to Portland cement: an overview, Constr. Build. Mater. 237 (2020) 117455, https://doi.org/10.1016/j.conbuildmat.2019.117455.
[18] M. Nawaz, A. Heitor, M. Sivakumar, Geopolymers in construction - recent developments, Constr. Build. Mater. 260 (2020) 120472, https://doi.org/10.1016/j.conbuildmat.2020.120472.
[19] J.L. Provis, Innovation in Cements—Can We Meet Future Construction Needs Sustainably? in: C. Ha-Minh, A.M. Tang, T.Q. Bui, X.H. Vu, D.V.K. Huynh (Eds.), CIGOS 2021 Emerg. Technol. Appl. Green Infrastruct. Springer Nature, Singapore, 2022, pp. 29–36, https://doi.org/10.1007/978-981-16-7160-9_2.
[20] J.L. Provis, J.S.J. Van Deventer (Eds.), Alkali Activated Materials: State-of-the-Art Report, RILEM TC 224-AAM, Springer Netherlands, Dordrecht, 2014, https://doi.org/10.1007/978-94-007-7672-2.
[21] S.A. Bernal, E.D. Rodríguez, A.P. Kirchheim, J.L. Provis, Management and valorisation of wastes through use in producing alkali-activated cement materials, J. Chem. Technol. Biotechnol. 91 (2016) 2365–2388, https://doi.org/10.1002/jctb.4927.
[22] J. Giro-Paloma, A. Maldonado-Alameda, J. Formosa, L. Barbieri, J.M. Chimenos, I. Lancellotti, Geopolymers based on the valorization of Municipal Solid Waste Incineration residues, IOP Conf. Ser. Mater. Sci. Eng. 251 (2017) 012125, https://doi.org/10.1088/1757-899X/251/1/012125.

[23] V. Medri, E. Landi, Recycling of porcelain stoneware scraps in alkali bonded ceramic composites, Ceram. Int. 40 (2014) 307–315, https://doi.org/10.1016/j.ceramint.2013.06.003.
[24] A. Natali Murri, V. Medri, E. Landi, Production and thermomechanical characterization of wool–geopolymer composites, J. Am. Ceram. Soc. 100 (2017) 2822–2831, https://doi.org/10.1111/jace.14853.
[25] H. Wu, C. Liang, D. Yang, Z. Ma, Development of sustainable geopolymer materials made with ground geopolymer waste powder as renewable binder up to 100, Constr. Build. Mater. 400 (2023) 132746, https://doi.org/10.1016/j.conbuildmat.2023.132746.
[26] Y. Zhang, C. Zhou, J. Song, J. Li, Y. Gong, Foundry waste reutilization: anti-shrinkage geopolymer based on nano-clay and coal gangue, Constr. Build. Mater. 434 (2024) 136710, https://doi.org/10.1016/j.conbuildmat.2024.136710.
[27] Z. Lei, S. Pavia, X. Wang, Biomass ash waste from agricultural residues: characterisation, reactivity and potential to develop one-part geopolymer cement, Constr. Build. Mater. 431 (2024) 136544, https://doi.org/10.1016/j.conbuildmat.2024.136544.
[28] G. D'Angelo, M. Fumo, M. del R. Merino, I. Capasso, A. Campanile, F. Iucolano, D. Caputo, B. Liguori, Crushed bricks: demolition waste as a sustainable raw material for geopolymers, Sustainability 13 (2021) 7572, https://doi.org/10.3390/su13147572.
[29] M. Alhawat, A. Ashour, G. Yildirim, A. Aldemir, M. Sahmaran, Properties of geopolymers sourced from construction and demolition waste: a review, J. Build. Eng. 50 (2022) 104104, https://doi.org/10.1016/j.jobe.2022.104104.
[30] D. Zaharaki, M. Galetakis, K. Komnitsas, Valorization of construction and demolition (C&D) and industrial wastes through alkali activation, Constr. Build. Mater. 121 (2016) 686–693, https://doi.org/10.1016/j.conbuildmat.2016.06.051.
[31] S. Dadsetan, H. Siad, M. Lachemi, M. Sahmaran, Construction and demolition waste in geopolymer concrete technology: a review, Mag. Concr. Res. 71 (2019) 1232–1252, https://doi.org/10.1680/jmacr.18.00307.
[32] X. Yu, M. Zhang, C. Li, K. Hayano, X. Kang, Synergistic effects of recycled demolition waste and GGBS-FA based geopolymers on the mechanical properties and stabilization mechanism of high plasticity clay, Case Stud. Constr. Mater. 20 (2024) e03261, https://doi.org/10.1016/j.cscm.2024.e03261.
[33] Z. Sun, H. Cui, H. An, D. Tao, Y. Xu, J. Zhai, Q. Li, Synthesis and thermal behavior of geopolymer-type material from waste ceramic, Constr. Build. Mater. 49 (2013) 281–287, https://doi.org/10.1016/j.conbuildmat.2013.08.063.
[34] L. Reig, M.M. Tashima, M.V. Borrachero, J. Monzó, C.R. Cheeseman, J. Payá, Properties and microstructure of alkali-activated red clay brick waste, Constr. Build. Mater. 43 (2013) 98–106, https://doi.org/10.1016/j.conbuildmat.2013.01.031.
[35] K. Komnitsas, D. Zaharaki, A. Vlachou, G. Bartzas, M. Galetakis, Effect of synthesis parameters on the quality of construction and demolition wastes (CDW) geopolymers, Adv. Powder Technol. 26 (2015) 368–376, https://doi.org/10.1016/j.apt.2014.11.012.
[36] R.A. Robayo-Salazar, J.F. Rivera, R. Mejía de Gutiérrez, Alkali-activated building materials made with recycled construction and demolition wastes, Constr. Build. Mater. 149 (2017) 130–138, https://doi.org/10.1016/j.conbuildmat.2017.05.122.
[37] M. Frías, R. Vigil de la Villa, S. Martínez-Ramírez, L. Fernández-Carrasco, E. Villar-Cociña, R. García-Giménez, Multi-technique characterization of a fine fraction of CDW and assessment of reactivity in a CDW/lime system, Minerals 10 (2020) 590, https://doi.org/10.3390/min10070590.
[38] D.O. de Lima, D.S. de Lira, M.F. Rojas, H.S. Junior, Assessment of the potential use of construction and demolition waste (CDW) fines as eco-pozzolan in binary and ternary cements, Constr. Build. Mater. 411 (2024) 134320, https://doi.org/10.1016/j.conbuildmat.2023.134320.
[39] J. Tan, J. De Vlieger, P. Desomer, J. Cai, J. Li, Co-disposal of construction and demolition waste (CDW) and municipal solid waste incineration fly ash (MSWI FA) through geopolymer technology, J. Clean. Prod. 362 (2022) 132502, https://doi.org/10.1016/j.jclepro.2022.132502.
[40] P. Rovnaník, B. Řezník, P. Rovnaníková, Blended alkali-activated fly ash / brick powder materials, Procedia Eng. 151 (2016) 108–113, https://doi.org/10.1016/j.proeng.2016.07.397.
[41] M.F. Zawrah, R.A. Gado, N. Feltin, S. Ducourtieux, L. Devoille, Recycling and utilization assessment of waste fired clay bricks (Grog) with granulated blast-furnace slag for geopolymer production, Process Saf. Environ. Prot. 103 (2016) 237–251, https://doi.org/10.1016/j.psep.2016.08.001.
[42] A.G. Díaz, S. Bueno, L.P. Villarejo, D. Eliche-Quesada, Improved strength of alkali activated materials based on construction and demolition waste with addition of rice husk ash, Constr. Build. Mater. 413 (2024) 134823, https://doi.org/10.1016/j.conbuildmat.2023.134823.
[43] M. Alhawat, G. Yildirim, A. Ashour, E. Ozcelikci, A. Aldemir, M. Sahmaran, A study on the influencing parameters in developing construction and demolition waste-based geopolymer concretes and their sustainability assessment, Constr. Build. Mater. 426 (2024) 136143, https://doi.org/10.1016/j.conbuildmat.2024.136143.
[44] H. İlcan, A.O. Demirbaş, H. Ulugöl, M. Şahmaran, Low-alkaline activated construction and demolition waste-based geopolymers, Constr. Build. Mater. 411 (2024) 134546, https://doi.org/10.1016/j.conbuildmat.2023.134546.
[45] M. Panizza, M. Natali, E. Garbin, S. Tamburini, M. Secco, Assessment of geopolymers with Construction and Demolition Waste (CDW) aggregates as a building material, Constr. Build. Mater. 181 (2018) 119–133, https://doi.org/10.1016/j.conbuildmat.2018.06.018.
[46] P. Rovnaník, P. Rovnaníková, M. Vyšvařil, S. Grzeszczyk, E. Janowska-Renkas, Rheological properties and microstructure of binary waste red brick powder/metakaolin geopolymer, Constr. Build. Mater. 188 (2018) 924–933, https://doi.org/10.1016/j.conbuildmat.2018.08.150.
[47] O. Mahmoodi, H. Siad, M. Lachemi, S. Dadsetan, M. Sahmaran, Development of ceramic tile waste geopolymer binders based on pre-targeted chemical ratios and ambient curing, Constr. Build. Mater. 258 (2020) 120297, https://doi.org/10.1016/j.conbuildmat.2020.120297.
[48] S. Dadsetan, H. Siad, M. Lachemi, M. Sahmaran, Extensive evaluation on the effect of glass powder on the rheology, strength, and microstructure of metakaolin-based geopolymer binders, Constr. Build. Mater. 268 (2021) 121168, https://doi.org/10.1016/j.conbuildmat.2020.121168.
[49] I. Giannopoulou, P.M. Robert, K.-M. Sakkas, M.F. Petrou, D. Nicolaides, High temperature performance of geopolymers based on construction and demolition waste, J. Build. Eng. 72 (2023) 106575, https://doi.org/10.1016/j.jobe.2023.106575.
[50] I. Giannopoulou, P.M. Robert, M.F. Petrou, D. Nicolaides, Mechanical behavior of construction and demolition waste-based alkali activated materials exposed to fire conditions, Constr. Build. Mater. 415 (2024) 134994, https://doi.org/10.1016/j.conbuildmat.2024.134994.
[51] Y. Chen, Study on the mechanical behavior of construction and demolition waste-based geopolymers under high-temperature conditions, J. Asian Archit. Build. Eng. (2024) 1–16, https://doi.org/10.1080/13467581.2024.2308595.
[52] M.E. Maciá, Á. Castillo, I. Martinez, F.J. Rubiano, High-temperature residual compressive strength in concretes bearing construction and demolition waste (CDW): an experimental study, Iran. J. Sci. Technol. Trans. Civ. Eng. 46 (2022) 4303–4312, https://doi.org/10.1007/s40996-022-00895-w.
[53] V. Medri, E. Papa, J. Lizion, E. Landi, Metakaolin-based geopolymer beads: production methods and characterization, J. Clean. Prod. 244 (2020) 118844, https://doi.org/10.1016/j.jclepro.2019.118844.
[54] J. Bochen, B. Słomka-Słupik, J. Ślusarek, Experimental study on salt crystallization in plasters subjected to simulate groundwater capillary rise, Constr. Build. Mater. 308 (2021) 125039, https://doi.org/10.1016/j.conbuildmat.2021.125039.
[55] H. Son, S.M. Park, J.H. Seo, H.K. Lee, Effect of $CaSO_4$ incorporation on pore structure and drying shrinkage of alkali-activated binders, Materials 12 (2019) 1673, https://doi.org/10.3390/ma12101673.
[56] D. Wang, Q. Wang, Z. Huang, New insights into the early reaction of NaOH-activated slag in the presence of $CaSO_4$, Compos. Part B Eng. 198 (2020) 108207, https://doi.org/10.1016/j.compositesb.2020.108207.
[57] V. Medri, S. Fabbri, J. Dedecek, Z. Sobalik, Z. Tvaruzkova, A. Vaccari, Role of the morphology and the dehydroxylation of metakaolins on geopolymerization, Appl. Clay Sci. 50 (2010) 538–545, https://doi.org/10.1016/j.clay.2010.10.010.
[58] C.K. Yip, J.L. Provis, G.C. Lukey, J.S.J. van Deventer, Carbonate mineral addition to metakaolin-based geopolymers, Cem. Concr. Compos. 30 (2008) 979–985, https://doi.org/10.1016/j.cemconcomp.2008.07.004.
[59] H. Xu, J.S.J. van Deventer, Factors affecting the geopolymerization of alkali-feldspars, Min. Metall. Explor. 19 (2002) 209–214, https://doi.org/10.1007/BF03403271.
[60] B. Kim, S. Lee, Review on characteristics of metakaolin-based geopolymer and fast setting, J. Korean Ceram. Soc. 57 (2020) 368–377, https://doi.org/10.1007/s43207-020-00043-y.
[61] A. Hamdan, H. Song, Z. Yao, M.F. Alnahhal, T. Kim, A. Hajimohammadi, Modifications to reaction mechanisms, phase assemblages and mechanical properties of alkali-activated slags induced by gypsum addition, Cem. Concr. Res. 174 (2023) 107311, https://doi.org/10.1016/j.cemconres.2023.107311.
[62] E. Landi, V. Medri, E. Papa, J. Dedecek, P. Klein, P. Benito, A. Vaccari, Alkali-bonded ceramics with hierarchical tailored porosity, Appl. Clay Sci. 73 (2013) 56–64, https://doi.org/10.1016/j.clay.2012.09.027.
[63] V. Medri, M.C. Marchioni, E. Landi, E. Papa, Development of membranes based on recycled geopolymer and zeolite through a cold sintering process, J. Eur. Ceram. Soc. (2024), https://doi.org/10.1016/j.jeurceramsoc.2024.05.053.
[64] UNI EN 13791:2019 - UNI Ente Italiano di Normazione, (n.d.). ⟨https://conto.uni.com/uni-en-13791-2019⟩ (accessed September 22, 2024).
[65] Z. Pavlík, J. Fořt, M. Pavlíková, J. Pokorný, A. Trník, R. Černý, Modified lime-cement plasters with enhanced thermal and hygric storage capacity for moderation of interior climate, Energy Build. 126 (2016) 113–127, https://doi.org/10.1016/j.enbuild.2016.05.004.
[66] H. Dong, P. Gao, G. Ye, Characterization and comparison of capillary pore structures of digital cement pastes, Mater. Struct. 50 (2017) 154, https://doi.org/10.1617/s11527-017-1023-9.
[67] P. Duxson, G.C. Lukey, J.S.J. van Deventer, Physical evolution of Na-geopolymer derived from metakaolin up to 1000 °C, J. Mater. Sci. 42 (2007) 3044–3054, https://doi.org/10.1007/s10853-006-0535-4.
[68] P. Duxson, G.C. Lukey, J.S.J. van Deventer, Thermal evolution of metakaolin geopolymers: Part 1 – physical evolution, J. Non-Cryst. Solids 352 (2006) 5541–5555, https://doi.org/10.1016/j.jnoncrysol.2006.09.019.
[69] E. Papa, V. Medri, E. Landi, B. Ballarin, F. Miccio, Production and characterization of geopolymers based on mixed compositions of metakaolin and coal ashes, Mater. Des. 56 (1980-2015) (2014) 409–415, https://doi.org/10.1016/j.matdes.2013.11.054.
[70] C.K. Yip, G.C. Lukey, J.S.J. van Deventer, The coexistence of geopolymeric gel and calcium silicate hydrate at the early stage of alkaline activation, Cem. Concr. Res. 35 (2005) 1688–1697, https://doi.org/10.1016/j.cemconres.2004.10.042.
[71] I. Lancellotti, M. Cannio, F. Bollino, M. Catauro, L. Barbieri, C. Leonelli, Geopolymers: an option for the valorization of incinerator bottom ash derived "end of waste, Ceram. Int. 41 (2015) 2116–2123, https://doi.org/10.1016/j.ceramint.2014.10.008.
[72] A. Natali Murri, W.D.A. Rickard, M.C. Bignozzi, A. van Riessen, High temperature behaviour of ambient cured alkali-activated materials based on ladle slag, Cem. Concr. Res. 43 (2013) 51–61, https://doi.org/10.1016/j.cemconres.2012.09.011.